




Article

Catalytic Evaluation of Nanoflower Structured Manganese Oxide Electrocatalyst for Oxygen Reduction in Alkaline Media

Siow Jing Han ¹, Mariam Ameen ^{1,2}, Mohamad Fahrul Radzi Hanifah ³ , Aqsha Aqsha ^{1,2}, Muhammad Roil Bilad ^{1,*} , Juhana Jaafar ³ and Soorathep Kheawhom ⁴ 

¹ Chemical Engineering Department, Universiti Teknologi PETRONAS, Bandar Seri Iskandar 32610, Perak, Malaysia; jhsio53095@gmail.com (S.J.H.); mariam.ameenkk@utp.edu.my (M.A.); aqsha@utp.edu.my (A.A.)

² HiCoE-Center for Biofuel and Biochemical Research, Institute of Self-Sustainable Building, Universiti Teknologi PETRONAS, Seri Iskandar 32610, Perak Darul Ridzuan, Malaysia

³ Advanced Membrane Technology Research Centre (AMTEC), Universiti Teknologi Malaysia (UTM), UTM Johor Bahru 81310, Johor, Malaysia; mfahrulradzi@gmail.com (M.F.R.H.); juhana@petroleum.utm.my (J.J.)

⁴ Center of Excellence in Process and Energy Systems Engineering, Department of Chemical Engineering, Faculty of Engineering, Chulalongkorn University, Bangkok 10330, Thailand; Soorathep.K@chula.ac.th

* Correspondence: mroil.bilad@utp.edu.my

Received: 27 May 2020; Accepted: 23 June 2020; Published: 23 July 2020



Abstract: An electrochemical nanoflowers manganese oxide (MnO₂) catalyst has gained much interest due to its high stability and high specific surface area. However, there are a lack of insightful studies of electrocatalyst performance in nanoflower MnO₂. This study assesses the electrocatalytic performances of nanoflower structure MnO₂ for both oxygen reduction reaction (ORR) and oxygen evolution reaction (OER) in a zinc–air battery as a bifunctional electrocatalyst. The prepared catalyst was characterized in term of morphology, crystallinity, and total surface area. Cyclic voltammetry and linear sweep voltammetry were used to evaluate the electrochemical behaviors of the as-prepared nanoflower-like MnO₂. The discharge performance test for zinc–air battery with a MnO₂ catalyst was also conducted. The results show that the MnO₂ prepared at dwell times of 2, 4 and 6 h were nanoflowers, nanoflower mixed with nanowires, and nanowires with corresponding specific surface areas of 52.4, 34.9 and 32.4 g/cm², respectively. The nanoflower-like MnO₂ catalyst exhibits a better electrocatalytic performance towards both ORR and OER compared to the nanowires. The number of electrons transferred for the MnO₂ with nanoflower, nanoflower mixed with nanowires, and nanowire structures is 3.68, 3.31 and 3.00, respectively. The as-prepared MnO₂ nanoflower-like structure exhibits the best discharge performance of 31% higher than the nanowires and reaches up to 30% of the theoretical discharge capacity of the zinc–air battery.

Keywords: manganese oxide electrocatalyst; metal–air battery; nanoflower structure; oxygen reduction reaction; oxygen evolution reaction

1. Introduction

Renewable energy sources have broadly attracted attention to supply global energy demand due to the excess utilization of petroleum-based fuels [1,2]. Nevertheless, the efficient utilization of renewable energy sources requires safe and cost-effective electricity storage systems. Zinc–air batteries are considered as the most promising alternative energy storage due to several advantages such as high theoretical specific energy density with a flat constant discharge voltage, the low reactivity of zinc, environmental safety and quick refueling with fresh zinc powder and granules. Moreover, the use of

highly abundant and free oxygen as the reactant at the cathode does not require a heavy casing to keep it inside which generally makes the battery heavy and space consuming [3–6].

However, the large overpotential (ΔV) between the oxygen evolution reaction (OER) and the oxygen reduction reaction (ORR) reduces the life cycle and, thus, limiting the performance of the secondary zinc–air batteries [7–12]. The development of efficient and stable bifunctional catalysts towards the OER and ORR is critical to support the technology developments.

Enormous researches have been conducted towards the development of high-performance batteries with low-cost materials [3,6]. Currently, the most used electrocatalyst for ORR and OER reactions is platinum. However, the high cost and susceptibility to catalyst poisoning has limited their commercialization in zinc–air batteries [13–21]. Hence, the search for an economical and viable catalyst with high catalytic performance as a potential component in zinc–air batteries has become the key for electrochemistry researchers.

The new development of effective and low-cost materials has been introduced for ORR such as nitrogen-doped graphene, which was synthesized by electrochemical exfoliation of commercial graphite in a Na_2SO_4 electrolyte with the addition of CaCO_3 as a separator of newly exfoliated FL-graphene sheets. Exfoliated FL-graphene was later infused with a suspension of green algae which worked as a nitrogen carrier. Impregnated FL-graphene was carbonized at a high temperature under the flow of nitrogen. This nitrogen-doped graphene has shown significant results for catalytic activity in ORR, which can be employed in a Zn–air battery [22].

Manganese oxide (MnO_2) is one of the most promising electrocatalysts since it has shown excellent electrocatalytic performances for OER and ORR under alkaline conditions [23–27]. Meanwhile, it is abundant in natural ores, low in toxicity, low cost and environmentally friendly. The catalytic activity of MnO_2 in its native form is low compared to the platinum and its group metals due to its weak O_2 binding ability and limited electronic conductivity [15,28,29]. However, the electrocatalytic performances of MnO_2 for ORR and OER is a highly structure sensitive. Therefore, the performance of MnO_2 catalysts can still be improved by modifying their morphologies, Mn valence state, preparation methods, crystalline phases and structures [30–32].

The nanoflower MnO_2 structure has gained much interest due to the high stability and high surface area to volume ratio [33]. Several studies have shown that the nanoflower structure exhibits the large surface area and can offer a significant improvement in ORR activities [34]. However, there are a lack of insightful studies of OER electrocatalyst properties on nanoflower MnO_2 , as well as its electrocatalytic performances. Hence, this study evaluates the electrocatalytic performances of nanoflower structure MnO_2 for both ORR and OER in the zinc–air battery as a bifunctional electrocatalyst.

2. Results

2.1. Morphological Study of the As-Prepared Catalysts

Figure 1 shows the SEM images for the synthesized MnO_2 catalysts with different dwell times. It shows that the rod-like MnO_2 structure was formed at a longer dwell time. This phenomenon can be explained by the Ostwald Ripening process during formation of the catalyst [23]. The nanoflower structure was produced in a dwell time of 2 h, nanoflower mixed with nanowires was produced in a dwell time of 4 h, and nanowires were produced in a dwell time of 6 h. The obtained nanoflower structure of the MnO_2 particles exhibits irregular shape with sizes ranging from 1 to 3 μm and all clumping together. Meanwhile, the nanowire morphology developed from one into a few microns' length, about 50 nm in diameter.

Figure 2 displays N_2 adsorption/desorption isotherms of all the catalysts, showing (from the slopes of the linear region of the curves) that the nanoflower MnO_2 has a higher specific surface area ($52.4 \text{ cm}^2/\text{g}$) followed by nanoflower mixed with nanowires ($34.9 \text{ cm}^2/\text{g}$) and nanowires ($32.4 \text{ cm}^2/\text{g}$). The results indicate that the nanoflower structure exhibits a higher surface area compared to nanowires. Therefore, more abundant nanoflower structures are present on the surface of the catalyst. This general

statement suggests that the higher surface is mainly responsible for higher catalytic performance for all types of catalysts, regardless of the type of metals and support [34]. The surface area varies from material to material and depends on preparation methods. In this study, a higher surface area was observed in nanoflower MnO_2 , which is a significant factor for high catalytic performance.

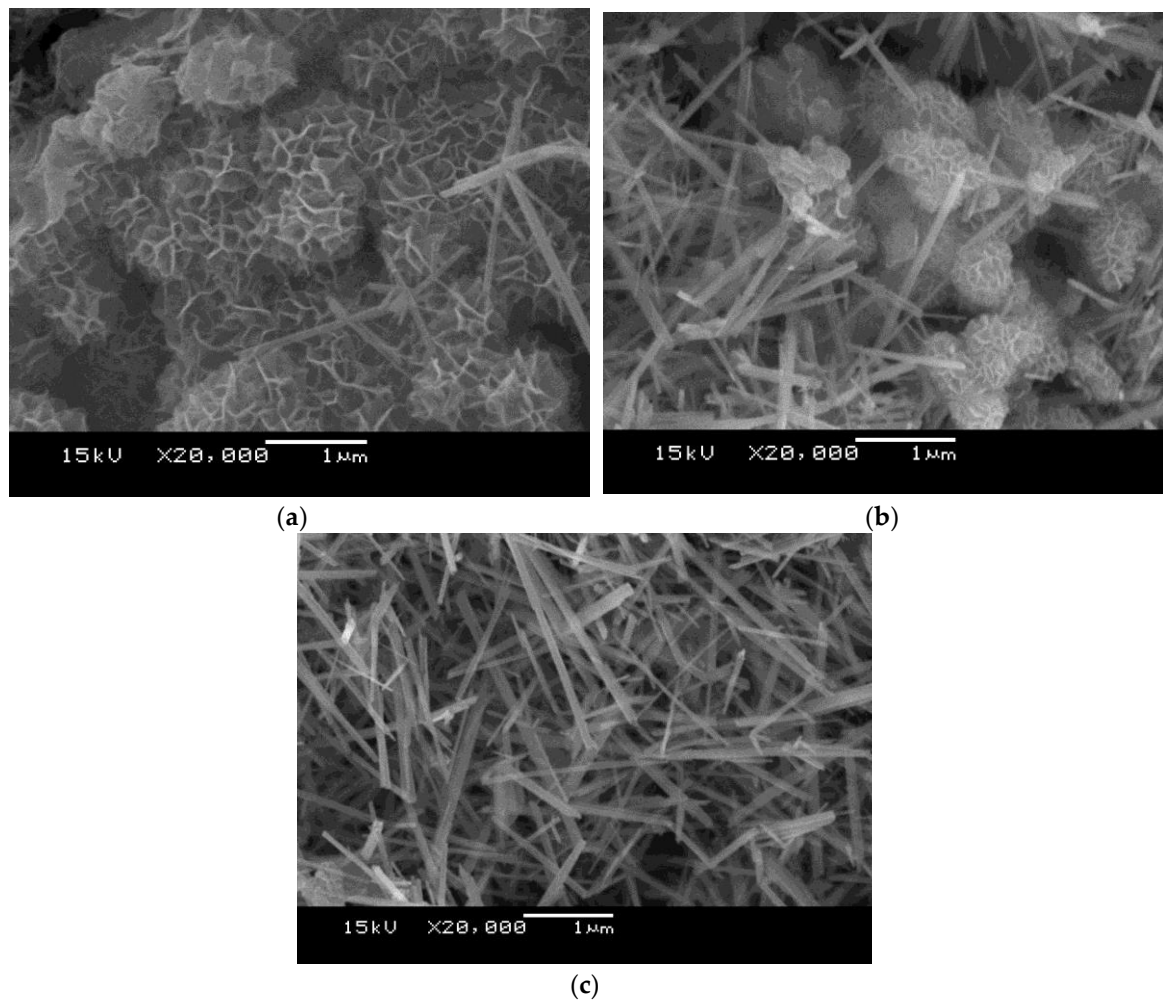


Figure 1. SEM images of synthesized MnO_2 with 2 (a), 4 (b), and 6 h (c) dwell time.

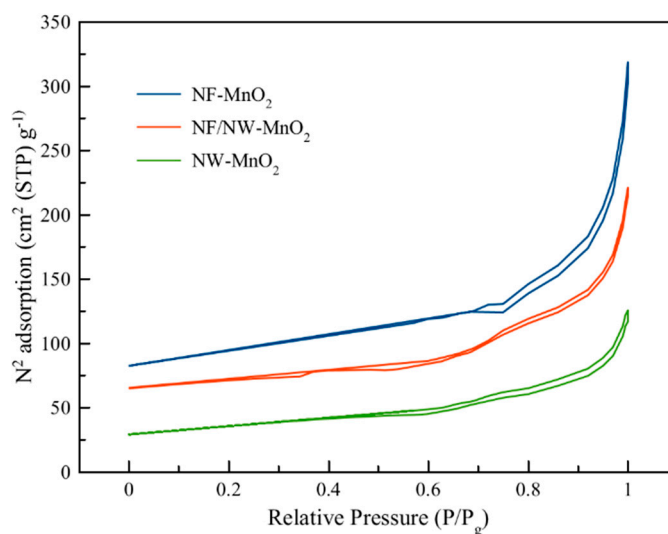


Figure 2. N_2 adsorption/desorption isotherms of all the samples.

2.2. Electrochemical Properties of the As-Prepared Catalysts

ORR is a complex and multi-electron reaction. The ORR can proceed via two different reaction pathways, namely, a direct four-electron pathway, as shown in Equation (1), or a two-electron pathway, as exhibited in Equations (2) and (3) [35].

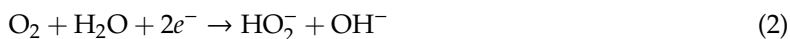


Figure 3 shows all the samples have a small but observable peak around -0.4 to -0.5 V vs. Ag/AgCl. This position of the reduction peak is close to the reduction potential of four-electron ORR. The findings indicate that all the samples tend to go for the four-electron ORR that does not produce hydrogen peroxide (HO_2^-). A further reduction of HO_2^- to OH^- was also not observed at around -1.0 V. Moreover, the carbon Vulcan XC 72 has, overall, a higher reduction peak compared to all the MnO_2 catalysts, which can be ascribed due to the low electrical conductivity of the MnO_2 .

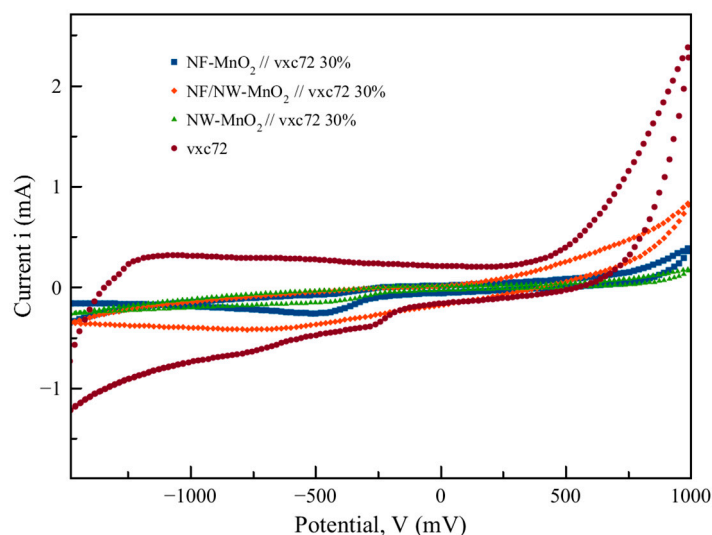


Figure 3. Cyclic voltammetry of pure carbon Vulcan XC 72, Nanoflower-like MnO_2 , nanoflower–nanowire-like MnO_2 , nanowire-like MnO_2 in O_2 saturated with 0.1-M KOH at a 50-mV/s scan rate.

2.3. Oxygen Reduction Reaction Performance

To further investigate the number of electron transferred and ORR performance of the catalyst, a linear sweep voltammetry (LSV) was conducted to obtain the polarization curves at different rotational speed in 0.1-M oxygen-saturated KOH for all the samples. Figure 4 demonstrates the polarization curves of all samples at 1600 rpm. It clearly shows that the onset potential and terminal current density of the prepared catalysts are both strongly influenced by the nanostructure. The carbon Vulcan XC 72/nanoflower-like MnO_2 has the highest terminal current density (-6.65 mA/cm^2) at a potential of -1.0 V and a higher onset potential (-0.13 V) at 1 mA/cm^2 . The carbon Vulcan XC 72/nanoflower-like MnO_2 catalyst has the highest performance followed by carbon Vulcan XC 72 mixed with major nanoflower and minor nanowires, carbon Vulcan XC 72 mixed with major nanowires and minor nanoflower, pure carbon Vulcan XC 72 and carbon Vulcan XC 72/commercial MnO_2 . This trend indicates that the nanoflower-like is better than the nanowire-like structure due to its higher specific surface area that provides more abundant active sites for the ORR.

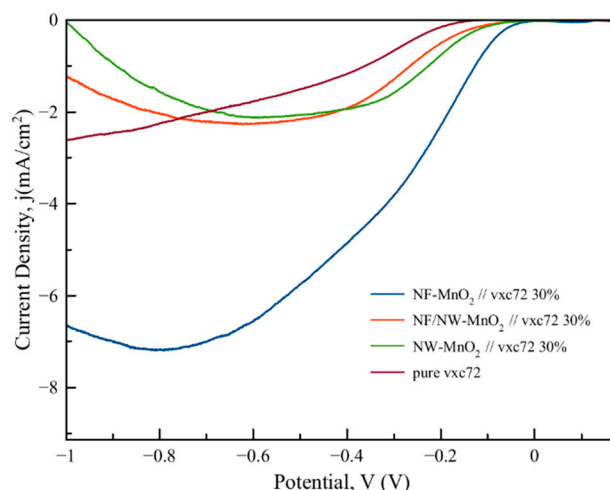


Figure 4. Linear sweep voltammetry curves of all prepared MnO₂ catalysts.

The number of electrons transferred per oxygen molecule for oxygen reduction was further evaluated by using the Koutecky–Levich (K-L) equation to study the ORR mechanism of the synthesized catalysts. The K-L equation is shown accordingly in Equations (4) and (5):

$$\frac{1}{j} = \frac{1}{j_k} + \frac{1}{B\omega^{1/2}} \quad (4)$$

$$B = 0.2nFD_{O_2}^{2/3}v^{-1/6}C_{O_2} \quad (5)$$

Figure 5 shows the K-L plot for carbon Vulcan XC 72/nanoflower-like MnO₂, carbon Vulcan XC 72/nanoflower–nanowire-like MnO₂, and carbon Vulcan XC 72/nanowire-like MnO₂ catalysts. It shows that as the potential increase, the gradient of the K-L plot which also refers as the number of electrons transferred decreases. The linear and parallel behavior of these plots indicate the first-order kinetics with respect to molecular oxygen for the ORR [29].

The number of electrons transferred for ORR reaction obtained from the K-L plot for the Vulcan XC 72/nanoflower-like MnO₂, carbon Vulcan XC 72/nanoflower-nanowire-like MnO₂ and Vulcan XC 72/nanowire-like MnO₂ catalysts are 3.68, 3.6 and 2.98 at −1.0 V, −0.8 V and −0.6 V, respectively. This result indicates that the synthesized nanoflower-like MnO₂ exhibits excellent electrocatalytic performance and stability at higher potentials. Meanwhile, the carbon Vulcan XC 72, mixed with major nanoflower and minor nanowires, and the carbon Vulcan XC 72, mixed with major nanowires and minor nanoflower, exhibit a similar trend as the carbon Vulcan XC 72/nanoflower-like MnO₂ but differ in the number of electrons transferred.

When comparing the K-L Plot of all samples at a fixed potential of −1.0 V and by obtaining the number of electrons transferred from the gradient of the K-L plot, the number of electrons transferred for carbon VXC 72 mixed with nanoflower MnO₂, carbon Vulcan XC 72 mixed with nanoflower mixed with nanowires, and carbon VXC 72 mixed with nanowires is 3.68, 3.31 and 3.00, respectively.

In order to suppress the evolution of hydrogen peroxide, the desired ORR pathway is the four-electron pathway in which the number of electrons transferred experimentally must be between two and four to show that the electrocatalyst promotes some of the ORR pathways to occur in the four-electron pathway. The results show that MnO₂ nanoflower has the best electrocatalyst performance towards the ORR, as the number of transferred electrons is close to four, suggesting the likelihood of promoting the ORR reaction toward the four-electron pathway. Meanwhile, the electrocatalytic performance for carbon Vulcan XC 72 mixed with major nanoflower and minor nanowires and carbon Vulcan XC 72 mixed with major nanowires and minor nanoflower are also within the acceptable range of two to four.

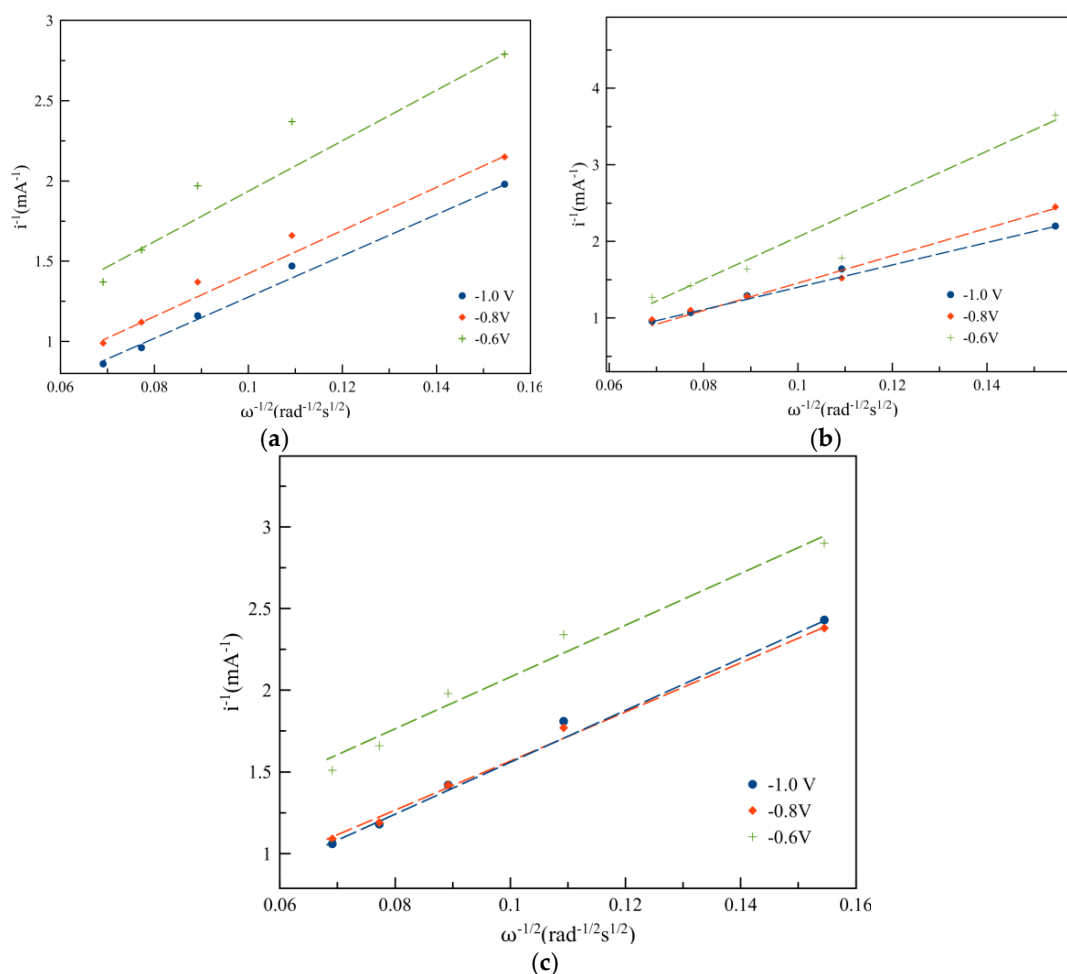


Figure 5. Koutecky–Levich plot for (a) nanoflower-like MnO_2 , (b) nanoflower–nanowire-like MnO_2 and (c) nanowire-like MnO_2 /carbon Vulcan XC 72 electrode at the various potentials.

2.4. Oxygen Evolution Reaction

As the MnO_2 has potential as a bifunctional catalyst towards OER, the OER performance of the nanostructure MnO_2 was further investigated. An LSV from 0.2 V to 1.0 V was conducted to obtain the polarization curves for the OER on rotating disk electrode as shown in Figure 6. The results confirm that the nanoflower-like MnO_2 has the lowest onset potential. The onset potential and the overpotential of the samples are summarized in Table 1.

Table 1 shows that the nanoflower-like MnO_2 has the lowest onset potential. As overpotential is defined as the difference between the theoretical half-reaction reduction potential of OER and the onset potential (which is 0.3244 V), the trend of the overpotential is the same as the onset potential. At lower overpotential, the energy lost during the reaction in the electrode is also lower. As shown in Table 1, the pure carbon VXC 72 has the highest overpotential (energy lost) during OER, while the nanoflower MnO_2 has the least energy lost. The difference in overpotential between MnO_2 and pure carbon VXC 72 can be explained by the electrocatalyst behaviors of the MnO_2 , where the hydroxide ions can be adsorbed on the surface of MnO_2 due to the valence state of MnO_2 . Such a phenomenon can be observed in Figure 6, which shows that the sharp increment in the current density (indicating the OER for MnO_2 samples and pure carbon VXC 72) has significant differences. The electrocatalyst behaviors of MnO_2 increases the rate of reaction and alters the pathway for the OER. Therefore, a higher gradient of the faradaic region from 0.7 to 1.0 V can be observed for the MnO_2 samples. Overall, the results suggest that the nanoflower structure has a better nanostructure with a higher stability and better electrocatalyst performance at a high potential.

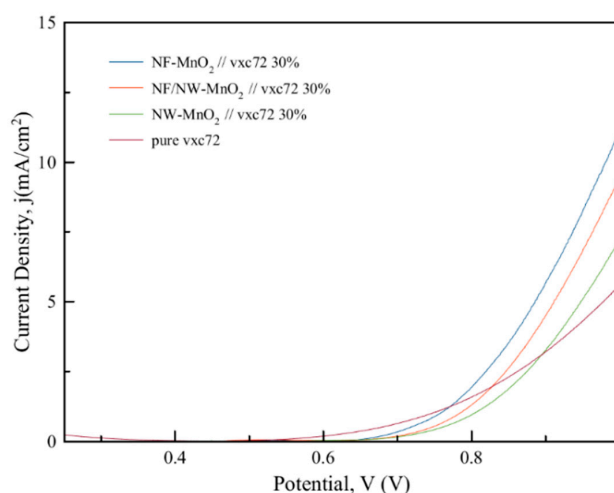


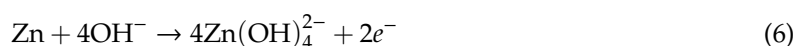
Figure 6. Linear sweep voltammetry curves for OER at 1600 rpm from 0.2 V to -1.0 V at the scan rate of 5 mV/s. (vxc72: Vulcan XC 72).

Table 1. Onset potential and overpotential for all the catalysts and pure carbon Vulcan XC 72.

Sample	Onset Potential at 5 mA/cm ² , V	Overpotential, V
NF-MnO ₂ //Vulcan XC 72 30%	0.89	0.57
NF/NW-MnO ₂ //Vulcan XC 72 30%	0.91	0.59
NW-MnO ₂ //Vulcan XC 72 30%	0.95	0.63
Vulcan XC 72	0.98	0.66

2.5. Zinc–Air Battery Discharge Performance

During discharge, at the anode, the zinc electrode reacts with hydroxide ion (OH[−]) and oxidize to form zincate ion Zn(OH)₄^{2−}, shown in Equation (6). Consequently, the precipitation of zinc oxide (ZnO) takes place when the dissolved zincate ion saturates and reaches its solubility, as shown in Equation (7).



At the cathode, the oxygen reduction reaction (ORR) occurs via four-electron (Equation (1)) or two-electron (Equations (2) and (3)) pathways. ORR consumes oxygen (O₂) and water (H₂O) and simultaneously produces a hydroxide ion. The hydroxide ion and water then transfers across the cell. Normally, the ORR kinetics are sluggish, and an ORR electrocatalyst is required to enhance ORR activity and battery performance. In alkaline solution, platinum (Pt) is an excellent ORR electrocatalyst, having excellent stability and showing a four-electron pathway. Nonetheless, its high cost hinders its practical applications. MnO₂ is a good alternative because it is significantly cheaper and more abundant than platinum.

The performances of the synthesized nanostructure MnO₂ as a catalyst in the cathode are presented in Figure 7. The galvanostatic discharge profiles indicate that the nanostructure MnO₂ follows the expected electrochemical behavior from the electrochemical characterization. In all cases, the batteries exhibited flat discharge profiles, having a voltage plateau at around 1.25 V. The Vulcan XC 72/nanoflower-like MnO₂ has the highest specific discharge capacity of up to 240 mAh/g zinc corresponding to a 31% higher performance than the nanowire-like MnO₂ in terms of discharge capacity. However, the theoretical specific discharge capacity of a zinc–air battery is 819 mAh/g, suggesting that the nanoflower-like MnO₂ only achieves 30% of the theoretical value, while the nanowire-like MnO₂ only achieves up to 20%. Such a phenomenon might be contributed to by the passivation that occurred on the zinc anode that usually exists in a zinc–air coin cell battery.

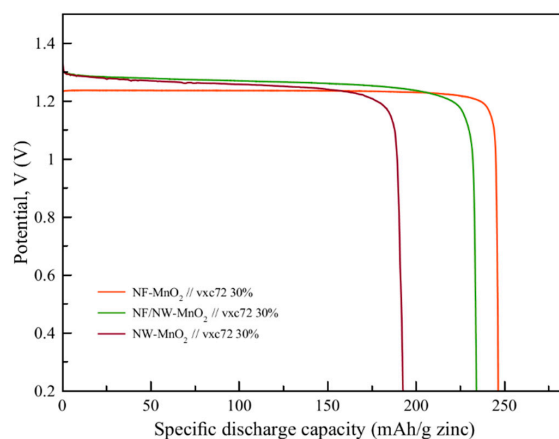


Figure 7. Galvanostatic discharge profiles of the Vulcan XC 72/commercial MnO₂, Vulcan XC 72/nanoflower-like MnO₂, Vulcan XC 72 mixed with major MnO₂ and minor manganese wires and Vulcan XC 72 mixed with major nanowires and minor nanoflower at a constant discharge current of 5 mA. (vxc72: Vulcan XC 72).

3. Discussion

MnO₂ can exist in various crystal structures, such as α -, β -, γ -, δ - and λ -MnO₂, depending on the way in which the MnO₆ octahedral unit shares their edges and corners. In δ -MnO₂, all MnO₆ octahedra are edge sharing, however, they are corner sharing in α -MnO₂. δ -MnO₂ has a layered structure and shows a nanoflower-like architecture, whilst α -MnO₂ has a tunnel structure and exhibited architecture of nanowires [36]. The SEM images of the MnO₂ catalysts, shown in Figure 1, indicate that the rod-like MnO₂ structure was formed at longer dwell time, indicating that the catalyst formation follows the Ostwald Ripening process [23]. In this process, smaller particles gain thermodynamic stability by depositing on a larger particle to minimize the surface area to volume ratio. Hence, as the reaction time increased larger nanostructures were formed, leading to a smaller surface area. The N₂ adsorption/desorption data suggest that nanostructure electro-catalysts improve electronic and catalytic properties due to the higher surface area, i.e., (52.4 cm²/g) compared to other counterparts such as nanoflower mixed with nanowires (34.9 cm²/g) and nanowires (32.4 cm²/g), offering more active reaction sites as proven from the highest anodic and cathodic current peaks of the Vulcan XC 72/nanoflower-like MnO₂, which correlates well with the high performances in ORR and OER owing to its highest specific surface area. This claim is confirmed by the data of the linear sweep voltammetry curves in Figure 4.

The results on the number of electrons transferred for the ORR reaction obtained from the K-L plot for different MnO₂ structures confirm that the synthesized nanoflower-like MnO₂ exhibits excellent electrocatalytic performance and stability at higher potentials, as also proven by the K-L plot. It shows that the MnO₂ nanoflower has the highest number of electrons transferred towards the four-electron pathway on the ORR. The results can be explained by the specific surface area of the synthesized MnO₂. A higher specific surface area leads to more active sites for reaction, ascribing the superiority of the nanoflower-like MnO₂ over the other structures, as also shown by the Onset potential and overpotential in Table 1.

Table 2 compares the performance of the MnO₂ catalysts developed in this study with other MnO₂ catalysts reported in the literature. The results obtained in the study are somewhat in line with earlier report. Despite showing a similar structure (nanoflower) and lower surface area, the number of electrons transferred for ORR is slightly higher than the reference [29]. It shows that the nanoflower-like MnO₂ poses surface area close to the nanorod- and nanoflake-like catalysts developed via the electrosynthesis method [20]. Despite showing a lower surface area, it shows higher electrons transferred for ORR from K-L plot. It is also worth noting that there is consistency in the data of the literature on the positive impact of the nanoflower structure in enhancing surface area, but this does not always positively correlate with the number of electrons transferred for the ORR.

Table 2. Summary of the ORR and OER parameters of recently reported nanostructure manganese oxide catalyst.

Catalyst	Nanostructure	Electrolyte and Reference Electrode	Synthesizing Method	BET Surface Area (m ² /g)	Overpotential for ORR (mV) at −0.1 mA/cm ²	Electrons Transferred for ORR from K-L Plot	Cathodic Tafel Slope (mV dec ^{−1})	Overpotential for OER (mV) at Specific Density	Anodic Tafel Slope (mV dec ^{−1})	Ref.
α-MnO ₂	Nanoflower	0.1 M KOH and Ag/AgCl	Hydrothermal	52.4	−0.570	3.68	-	0.89 at 5 mA/cm ²	-	This study
α-MnO ₂	Nanoflower/ Nanowires			34.9	−0.590	3.31	-	0.91 at 5 mA/cm ²	-	
α-MnO ₂	Nanowires			32.4	−0.530	3.00	-	0.95 at 5 mA/cm ²	-	
α-MnO ₂	Nanoflower	0.1 M KOH and Ag/AgCl	Hydrothermal	68.3	−0.302	3.7	-	-	-	[15]
α-MnO ₂	Nanowires			40.1	−0.500	3.87	-	-	-	
α-MnO ₂	Nanowires			27.7	−0.616	3.5	65	-	-	
α-MnO ₂	Nanotubes	0.1 M KOH and SCE	Hydrothermal	21.1	−0.586	3.0	90	-	-	[29]
α-MnO ₂	Nanoparticles			34.7	−0.736	2.3	90	-	-	
α-MnO ₂	Nanorod			24.8	−0.606	3.2	65	-	-	
α-MnO ₂	Nanoflower			32.4	−0.876	1.9	115	-	-	
β-MnO ₂	Nanorod	0.1 M KOH and Ag/AgCl	Hydrothermal	37.9	−0.75	-	-	-	-	[37]
α-MnO ₂	Nanorod	0.1 M KOH and Ag/AgCl	Electrosynthesis	59.58	−0.351	2.23	-	-	-	[20]
α-MnO ₂	Nanoflakes			59.58	−0.651	1.75	-	-	-	
β-MnO ₂	Nanorod	0.1 M KOH and SCE	Solid state method	5	−0.551	2.4	-	0.6 at 10 mA/cm ²	180.2	[21]
δ-MnO ₂	Nanoflower		Hydrothermal	26	−0.701	1.7	-	0.75 at 10 mA/cm ²	188.6	
Porous Mn ₂ O ₃	Nanoplates	0.1 M KOH and Hg/HgO	Wet-chemical	-	-	-	-	-	81	[25]

4. Materials and Methods

4.1. Chemical and Materials

Analytical grade potassium permanganate (KMnO_4) (R&M Chemicals, London, UK) and Manganese (II) sulfate-i-hydrate ($\text{MnSO}_4 \cdot \text{H}_2\text{O}$) (Bendosen Laboratory Chemicals, Bendosen, Norway) were used to synthesize MnO_2 . KOH pellets (99%) and zinc sulphate ($\text{ZnSO}_4 \cdot 7\text{H}_2\text{O}$) (CT Chemical Co., Ltd., Bangkok, Thailand), were used to prepare the electrolytes for the electrochemical characterization and battery, respectively. Carbon black (Vulcan[®] XC 72, Cabot Corporation, Boston, MA, USA) was used to prepare the working electrode for electrochemical characterization. For the zinc–air coin cell battery fabrication, 1-mm-thick nickel foam with a purity of 99.97% (Qijing Trading Co., Ltd., Bangkok, Thailand) was used as the current collector for the cathode. Carbon BP2000 (Black Pearls 2000, Cabot Corporation) and Polystyrene-co-butadiene binder (5%, Sigma-Aldrich, St. Louis, MO, USA) and toluene solvent (99.8%, QReC, Selangor, Malaysia) were used to prepare the hydrophilic catalyst layer of the cathode, while poly(tetrafluoroethylene) (PTFE powder, 1 μm , Sigma-Aldrich, St. Louis, MO, USA) was used as a binder to prepare the air diffusion layer of cathode. Carbopol (940) with a molecular weight of approximately 1450 monomer units, Whatman filter paper No.1 (Sigma-Aldrich, St. Louis, MO, USA) and poly (vinyl acetate) (PVAC) (TOA Paint Public Co., Ltd., Samutprakan, Thailand) were used in fabrication of separator for zinc–air coin cell. The standard CR2032 Stainless steel coin cell parts with 20 holes drilled at the coin cell top is used as the casing of the coin cell.

4.2. Synthesis of Nanoflower-Like MnO_2 Catalyst

The nanoflower-like MnO_2 was synthesized using hydrothermal synthesis. Separately, 0.1 g of $\text{MnSO}_4 \cdot \text{H}_2\text{O}$ and 0.25 g of KMnO_4 were dissolved in 25 mL of deionized water and the solutions were mixed and transferred into a 100-mL, Teflon-lined, stainless-steel autoclave and heated at 140 °C in an oil bath or oven for 2 h. The autoclave was cooled down to room temperature and then the excess solution was filtered. Lastly, the obtained MnO_2 powder was washed with ethanol and water and dried in an oven at 60 °C for overnight. The synthesis was repeated with different reaction times for 4 and 6 h to obtain the different nanostructures of MnO_2 .

4.3. Characterization

The obtained samples were characterized by Scanning electron microscopy (SEM, JEOL-JSM-6480) to investigate the nanostructure of the MnO_2 . Brunauer–Emmett–Teller (BET) specific surface areas of the samples were determined from nitrogen adsorption isotherms that were performed on a BEL Japan BELSORP-mini II.

4.4. Electrochemical Measurement

All electrochemical measurements were carried out in a three-electrode configuration by a potentiostat/galvanostat with an impedance measurement unit (AMETEK, PAR VersaSTAT 3A). The standard three-electrode cell consists of platinum foil as the counter electrode, a Ag/AgCl electrode as a reference electrode, and a modified glassy carbon electrode (GCE) as the working electrode. The electrocatalytic activity of the as-prepared catalysts towards ORR was measured by cyclic voltammogram (CV) in a mixture of 0.1-M KOH at a scan rate of 50 mV s^{-1} from -1.8 to 1 V under an ambient atmosphere. For the ORR, Linear Sweep Voltammetry (LSV) was applied with a scan rate of 1 mV/s from 0.2 to -1 V, with the cathodic traces set at a rotational speed of 0, 400, 800, 1200, 1600 and 2000 RPM. For OER, the LSV was applied with a scan rate of 1 mV/s from 0.2 to 1 V, with the anodic traces set at rotational speeds of 0, 400, 800, 1200, 1600 and 2000 RPM.

4.5. Preparation of Working Electrode

In a typical procedure, 0.5 g of the nanoflower-like MnO_2 catalysts were ultrasonically mixed in 1 mL 5% polyvinylidene fluoride (PVDF) solutions to form homogenous catalyst ink under room condition. Then, 0.05 mL of the catalyst ink was dripping onto the surface of the glassy carbon electrode (GCE) attached to the rotary machine using a micropipette and then dried at room temperature.

4.6. Electrode and Battery Fabrication

Zinc–air coin cell batteries were fabricated and used to evaluate the discharge capacity of batteries with different catalysts. The fabricated coin cell consisted of three main parts: cathode, anode, and separator. The cathode was synthesized by coating carbon ink solution on a nickel foam. One side of the nickel foam (exhibited hydrophilic properties for reaction occur in the electrolyte) was coated with carbon homogeneous ink solution which consisted of 30 wt.% MnO_2 , 70 wt.% carbon Vulcan XC 72, and 2.5 wt.% of (MnO_2 /carbon) dissolved in toluene. Another side of the nickel (exhibited hydrophobic properties as an air diffusion layer) was coated with carbon homogeneous ink solution consisted of 40 wt.% of carbon Vulcan XC 72, 40 wt.% Polytetrafluoroethylene (PTFE), 20% glucose and ethanol were used as the solvent. The anode was prepared by zinc electroplating in 500 cm³ of 1-M $\text{ZnSO}_4 \cdot 7\text{H}_2\text{O}$ solution on the surface of the nickel foam. Nickel foams with dimensions of $10 \times 1 \times 0.1$ cm were placed vertically, in parallel at the opposite side of the zinc plate in the electrolyte. The electrodes were connected to a digital DC power supply (ATTEN APS 3005s) operated at galvanostatic mode at voltage of 1.6 V for 2 h for each side of the nickel foam. The separator was a solid polymer electrolyte (SPE) prepared homogeneously by mixing 0.6 g of Carbopol 940 and 15 g of PVAC in 40 mL of deionized water and 15 mL of 7-M KOH solution using a homogenizer. The prepared Carbopol solution was then transferred into a petri dish and dried at open air for 2 to 3 days. The obtained SPE should be around 0.1 to 0.2 mm. After the cathode, anode and separator were ready, a coin cell battery was set up according to the schematic diagram shown in Figure 8. The assembled coin-cell stack was then pressed under 100 kg/cm^2 using hydraulic presser.

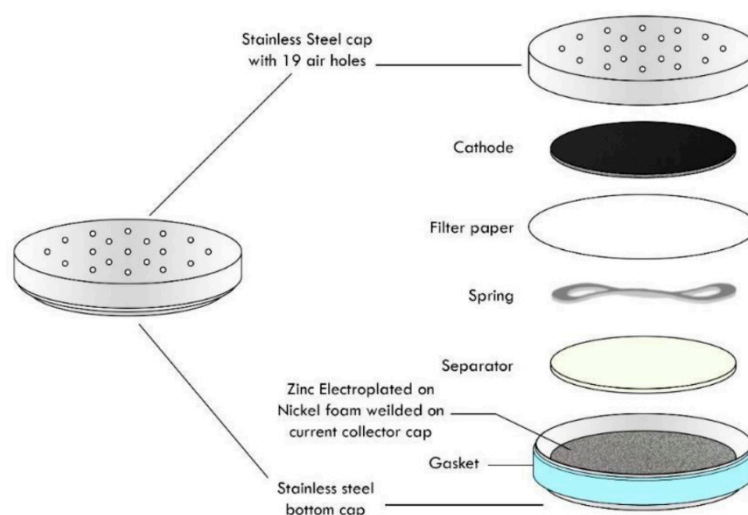


Figure 8. Schematic diagram of the coin cell battery.

4.7. Battery Performance Test

The prepared coin cell was connected to a coin cell battery tester, Netware (TOB-CT-4008-5V10mA-164), and discharged at a discharge current of 5 mA until the potential of coin cell depleted below the cut-off voltage of 0.01 V. The specific discharge capacity was obtained by divide the mass of zinc electroplated on the nickel foam which required to measure and record every time before setting up the coin cell.

5. Conclusions

The nanoflower-like MnO₂ catalyst structure was successfully prepared by the hydrothermal method. The formation of such structure was confirmed from the SEM shows image in which the dwell times of 2, 4 and 6 h resulting in nanoflowers, nanoflower mixed with nanowires and nanowires structures, respectively. BET results confirm that the nanoflower poses the highest specific surface area of 52.4 cm²/g followed by nanoflower mixed with nanowires of 34.9 cm²/g and nanowires of 32.4 cm²/g. The ORR and OER LSV polarization curve prove the hypothesis of the high performance of nanoflower MnO₂ due to its large specific surface area. In terms of ORR, the number of electrons transferred for carbon VXC 72 mixed with nanoflower MnO₂, carbon VXC 72 mixed with nanoflower mixed with nanowires and carbon VXC 72 mixed with nanowires are 3.68, 3.31 and 3.00, respectively. The synthesized MnO₂ has an excellent coin cell battery performance on improving the discharge capacity of a zinc–air battery. Among all the samples, nanoflower MnO₂ exhibits the best discharge performance, reaching up to 30% of the theoretical discharge capacity of the zinc–air battery.

Author Contributions: S.J.H. and M.R.B. conceived and designed the experiments; S.J.H. performed the experiments and wrote the paper, A.A. and M.A. helped to analyzed the data and format the paper; S.K. contributed in material supply and equipment support in their laboratory; M.F.R.H. and J.J. supported in software tools. All authors have read and agreed to the published version of the manuscript.

Funding: Authors acknowledge the Ministry of Higher Education Malaysia for providing Fundamental Research Grant and the APC (Cost Center: 015MA0-037, Reference Number: FRGS/1/2018/TK02/UTP/03/2).

Conflicts of Interest: The authors declare no conflict of interest.

References

1. Ameen, M.; Azizan, M.T.; Yusup, S.; Ramli, A.; Shahbaz, M.; Aqsha, A. Process optimization of green diesel selectivity and understanding of reaction intermediates. *Renew. Energy* **2020**, *149*, 1092–1106. [[CrossRef](#)]
2. Ameen, M.; Azizan, M.T.; Yusup, S.; Ramli, A.; Shahbaz, M.; Aqsha, A.; Kaur, H.; Wai, C.K. Parametric Studies on Hydrodeoxygenation of Rubber Seed Oil for Diesel Range Hydrocarbon Production. *Energy Fuels* **2020**, *34*, 4603–4617. [[CrossRef](#)]
3. Pei, P.; Wang, K.; Ma, Z. Technologies for extending zinc–air battery’s cyclife: A review. *Appl. Energy* **2014**, *128*, 315–324. [[CrossRef](#)]
4. Li, Y.; Dai, H. Recent advances in zinc–air batteries. *Chem. Soc. Rev.* **2014**, *43*, 5257–5275. [[CrossRef](#)]
5. Yang, D.; Zhang, L.; Yan, X.; Yao, X. Recent Progress in Oxygen Electrocatalysts for Zinc-Air Batteries. *Small Methods* **2017**, *1*, 1700209. [[CrossRef](#)]
6. Tijani, M.M.; Aqsha, A.; Yu, N.; Mahinpey, N. Determination of redox pathways of supported bimetallic oxygen carriers in a methane fuelled chemical looping combustion system. *Fuel* **2018**, *233*, 133–145. [[CrossRef](#)]
7. Mainar, A.R.; Colmenares, L.C.; Leonet, O.; Alcaide, F.; Iruin, J.J.; Weinberger, S.; Hacker, V.; Iruin, E.; Urdanpilleta, I.; Blazquez, J.A. Manganese oxide catalysts for secondary zinc air batteries: From electrocatalytic activity to bifunctional air electrode performance. *Electrochim. Acta* **2016**, *217*, 80–91. [[CrossRef](#)]
8. Mao, L.; Sotomura, T.; Nakatsu, K.; Koshiha, N.; Zhang, D.; Ohsaka, T. Electrochemical Characterization of Catalytic Activities of Manganese Oxides to Oxygen Reduction in Alkaline Aqueous Solution. *J. Electrochem. Soc.* **2002**, *149*, A504. [[CrossRef](#)]
9. Su, H.-Y.; Gorlin, Y.; Man, I.C.; Calle-Vallejo, F.; Nørskov, J.K.; Jaramillo, T.F.; Rossmeisl, J. Identifying active surface phases for metal oxide electrocatalysts: A study of manganese oxide bi-functional catalysts for oxygen reduction and water oxidation catalysis. *Phys. Chem. Chem. Phys.* **2012**, *14*, 14010. [[CrossRef](#)]
10. Tian, L.; Wang, J.; Wang, K.; Wo, H.; Wang, X.; Zhuang, W.; Li, T.; Du, X. Carbon-quantum-dots-embedded MnO₂ nanoflower as an efficient electrocatalyst for oxygen evolution in alkaline media. *Carbon* **2019**, *143*, 457–466. [[CrossRef](#)]
11. Yang, J.; Xu, J.J. Nanoporous amorphous manganese oxide as electrocatalyst for oxygen reduction in alkaline solutions. *Electrochem. Commun.* **2003**, *5*, 306–311. [[CrossRef](#)]
12. Yeager, E. Dioxygen electrocatalysis: Mechanisms in relation to catalyst structure. *J. Mol. Catal.* **1986**, *38*, 5–25. [[CrossRef](#)]

13. Calegario, M.L.; Lima, F.H.B.; Ticianelli, E.A. Oxygen reduction reaction on nanosized manganese oxide particles dispersed on carbon in alkaline solutions. *J. Power Sources* **2006**, *158*, 735–739. [[CrossRef](#)]
14. Cheng, F.; Chen, J. Metal–air batteries: From oxygen reduction electrochemistry to cathode catalysts. *Chem. Soc. Rev.* **2012**, *41*, 2172. [[CrossRef](#)] [[PubMed](#)]
15. Cheng, F.; Su, Y.; Liang, J.; Tao, Z.; Chen, J. MnO₂-Based Nanostructures as Catalysts for Electrochemical Oxygen Reduction in Alkaline Media[†]. *Chem. Mater.* **2010**, *22*, 898–905. [[CrossRef](#)]
16. Christensen, P.A.; Hamnett, A.; Linares-Moya, D. Oxygen reduction and fuel oxidation in alkaline solution. *Phys. Chem. Chem. Phys.* **2011**, *13*, 5206. [[CrossRef](#)]
17. Eftekhari, A. Tuning the electrocatalysts for oxygen evolution reaction. *Mater. Today Energy* **2017**, *5*, 37–57. [[CrossRef](#)]
18. Sweth, J.A.; Geetha, A.; Ramamurthi, K. Morphological and structural analysis of manganese oxide nanoflowers prepared under different reaction conditions. *Appl. Surf. Sci.* **2018**, *449*, 228–232. [[CrossRef](#)]
19. Liu, X.; Chen, C.; Zhao, Y.; Jia, B. A Review on the Synthesis of Manganese Oxide Nanomaterials and Their Applications on Lithium-Ion Batteries. *J. Nanomater.* **2013**, *2013*, 1–7. [[CrossRef](#)]
20. Mahmudi, M.; Widiyastuti, W.; Nurlilasari, P.; Affandi, S.; Setyawan, H. Manganese dioxide nanoparticles synthesized by electrochemical method and its catalytic activity towards oxygen reduction reaction. *J. Ceram. Soc. Jpn.* **2018**, *126*, 906–913. [[CrossRef](#)]
21. Meng, Y.; Song, W.; Huang, H.; Ren, Z.; Chen, S.-Y.; Suib, S.L. Structure–Property Relationship of Bifunctional MnO₂ Nanostructures: Highly Efficient, Ultra-Stable Electrochemical Water Oxidation and Oxygen Reduction Reaction Catalysts Identified in Alkaline Media. *J. Am. Chem. Soc.* **2014**, *136*, 11452–11464. [[CrossRef](#)] [[PubMed](#)]
22. Ilnicka, A.; Skorupska, M.; Romanowski, P.; Kamedulski, P.; Lukaszewicz, J.P. Improving the Performance of Zn-Air Batteries with N-Doped Electroexfoliated Graphene. *Materials* **2020**, *13*, 2115. [[CrossRef](#)]
23. Haoran, Y.; Lifang, D.; Tao, L.; Yong, C. Hydrothermal Synthesis of Nanostructured Manganese Oxide as Cathodic Catalyst in a Microbial Fuel Cell Fed with Leachate. *Sci. World J.* **2014**, *2014*, 1–6. [[CrossRef](#)]
24. Lima, F.H.B.; Calegario, M.L.; Ticianelli, E.A. Electrocatalytic activity of manganese oxides prepared by thermal decomposition for oxygen reduction. *Electrochim. Acta* **2007**, *52*, 3732–3738. [[CrossRef](#)]
25. Sim, H.; Lee, J.; Yu, T.; Lim, B. Manganese oxide with different composition and morphology as electrocatalyst for oxygen evolution reaction. *Korean J. Chem. Eng.* **2018**, *35*, 257–262. [[CrossRef](#)]
26. Valim, R.B.; Santos, M.C.; Lanza, M.R.V.; Machado, S.A.S.; Lima, F.H.B.; Calegario, M.L. Oxygen reduction reaction catalyzed by ε-MnO₂: Influence of the crystalline structure on the reaction mechanism. *Electrochim. Acta* **2012**, *85*, 423–431. [[CrossRef](#)]
27. Zhou, D.; Lü, X.; Liu, D. Electro-catalytic effect of manganese oxide on oxygen reduction at teflonbonded carbon electrode. *Trans. Nonferrous Met. Soc. China* **2006**, *16*, 217–222. [[CrossRef](#)]
28. Giménez, S. *Photoelectrochemical Solar Fuel Production*; Springer International Publishing: Berlin, Germany, 2016; ISBN 978-3-319-29641-8.
29. Selvakumar, K.; Senthil Kumar, S.M.; Thangamuthu, R.; Ganesan, K.; Murugan, P.; Rajput, P.; Jha, S.N.; Bhattacharyya, D. Physicochemical Investigation of Shape-Designed MnO₂ Nanostructures and Their Influence on Oxygen Reduction Reaction Activity in Alkaline Solution. *J. Phys. Chem. C* **2015**, *119*, 6604–6618. [[CrossRef](#)]
30. Chen, Y.; Hong, Y.; Ma, Y.; Li, J. Synthesis and formation mechanism of urchin-like nano/micro-hybrid α-MnO₂. *J. Alloys Compd.* **2010**, *490*, 331–335. [[CrossRef](#)]
31. Hashem, A.M.; Abdel-Ghany, A.E.; El-Tawil, R.; Bhaskar, A.; Hunzinger, B.; Ehrenberg, H.; Mauger, A.; Julien, C.M. Urchin-like α-MnO₂ formed by nanoneedles for high-performance lithium batteries. *Ionics* **2016**, *22*, 2263–2271. [[CrossRef](#)]
32. Rossouw, M.H.; Liles, D.C.; Thackeray, M.; David, W.I.F.; Hull, S. Alpha manganese dioxide for lithium batteries: A structural and electrochemical study. *Mater. Res. Bull.* **1992**, *27*, 221–230. [[CrossRef](#)]
33. Shende, P.; Kasture, P.; Gaud, R.S. Nanoflowers: The future trend of nanotechnology for multi-applications. *Artif. Cells Nanomed. Biotechnol.* **2018**, *46*, 413–422. [[CrossRef](#)] [[PubMed](#)]
34. Tahir, M.; Pan, L.; Idrees, F.; Zhang, X.; Wang, L.; Zou, J.-J.; Wang, Z.L. Electrocatalytic oxygen evolution reaction for energy conversion and storage: A comprehensive review. *Nano Energy* **2017**, *37*, 136–157. [[CrossRef](#)]

35. Poolnapol, L.; Kao-ian, W.; Somwangthanaroj, A.; Mahlendorf, F.; Nguyen, M.T.; Yonezawa, T.; Kheawhom, S. Silver Decorated Reduced Graphene Oxide as Electrocatalyst for Zinc–Air Batteries. *Energies* **2020**, *13*, 462. [[CrossRef](#)]
36. Corpuz, R.D.; De Juan-Corpuz, L.M.; Nguyen, M.T.; Yonezawa, T.; Wu, H.-L.; Somwangthanaroj, A.; Kheawhom, S. Binder-Free α -MnO₂ Nanowires on Carbon Cloth as Cathode Material for Zinc-Ion Batteries. *Int. J. Mol. Sci.* **2020**, *21*, 3113. [[CrossRef](#)] [[PubMed](#)]
37. Kumar, N.; Dineshkumar, P.; Rameshbabu, R.; Sen, A. Facile size-controllable synthesis of single crystalline β -MnO₂ nanorods under varying acidic strengths. *RSC Adv.* **2016**, *6*, 7448–7454. [[CrossRef](#)]



© 2020 by the authors. Licensee MDPI, Basel, Switzerland. This article is an open access article distributed under the terms and conditions of the Creative Commons Attribution (CC BY) license (<http://creativecommons.org/licenses/by/4.0/>).